Mon. Not. R. Astron. Soc. **362,** 1233–1246 (2005) doi:10.1111/j.1365-2966.2005.09384.x

Where are the stars?

V. R. Eke,[1⋆] C. M. Baugh,[1] Shaun Cole,[1] Carlos S. Frenk,[1] H. M. King[1] and John A. Peacock[2]

[1]*Department of Physics, University of Durham, South Road, Durham DH1 3LE*
[2]*Institute for Astronomy, University of Edinburgh, Royal Observatory, Blackford Hill, Edinburgh EH9 3HJ*

Accepted 2005 June 28. Received 2005 May 16; in original form 2004 December 2

ABSTRACT

The Two degree Field Galaxy Redshift Survey (2dFGRS) is used in conjunction with the Two Micron All-Sky Survey (2MASS) Extended Source Catalogue (XSC) to study the near-infrared light and stellar mass content of the local Universe. Mock galaxy catalogues, constructed from cosmological N-body simulations and semi-analytical galaxy formation models, are used to gauge the accuracy with which quantities can be recovered. The mean luminosity densities of the Universe are found to be $\bar{\rho}_J = (3.57 \pm 0.11) \times 10^8\, h\, \mathrm{L}_\odot\, \mathrm{Mpc}^{-3}$ and $\bar{\rho}_{K_\mathrm{S}} = (7.04 \pm 0.23) \times 10^8\, h\, \mathrm{L}_\odot\, \mathrm{Mpc}^{-3}$ (statistical uncertainty only, and not accounting for the 2MASS low surface brightness incompleteness). Using the 2dFGRS Percolation-Inferred Galaxy Group (2PIGG) catalogue, the group mass-to-light ratio in the K_S band is found to increase by a factor of $\sim$3 when going from groups with total b_J-band luminosities of $3 \times 10^{10}\, h^{-2}\, \mathrm{L}_\odot$ to the richest clusters. These clusters have typical dynamical mass-to-light ratios of $\Upsilon_K \approx 80\, h \Upsilon_\odot$. Galaxy luminosities are used to estimate stellar masses. Taking into account the bias introduced by uncertainties in estimating galaxy stellar masses, a value of $\Omega_\mathrm{stars} h = (1.11 \pm 0.05) \times 10^{-3}$ is measured, assuming that a Kennicutt stellar initial mass function (IMF) is applicable to all galaxies. Changing this to a Salpeter stellar IMF gives $\Omega_\mathrm{stars} h \approx 2.3 \times 10^{-3}$. The 2PIGGs are then used to study the distribution of the stellar content of the local Universe among groups of different size. The three main conclusions are: (1) a slowly rising stellar mass-to-K_S band light ratio is found with the clusters having the largest value of $\sim 0.5 \Upsilon_\odot$, (2) in contrast, the fraction of mass in stars decreases with increasing group size, reaching $\sim 5 \times 10^{-3}\, h$ for the rich clusters, and (3) in answer to the question posed in the title, most stellar mass is contained in Local Group-sized objects ($M \sim 2 \times 10^{12}\, h^{-1}\, \mathrm{M}_\odot$) with only $\sim$2 per cent in clusters with $M \gtrsim 5 \times 10^{14}\, h^{-1}\, \mathrm{M}_\odot$.

Key words: galaxies: clusters: general – galaxies: haloes – galaxies: stellar content – large-scale structure of Universe.

1 INTRODUCTION

Understanding the impact that environment has on a galaxy's ability to form stars is one of the main goals of cosmology. A very pertinent observational constraint is the manner in which stellar mass is distributed between galaxy systems of different size. This paper describes a measurement of this constraint, using a combination of the Two Micron All-Sky Survey (2MASS) Extended Source Catalogue (XSC) (Jarrett et al. 2000) and the Two degree Field Galaxy Redshift Survey (2dFGRS) (Colless et al. 2001, 2003) Percolation-Inferred Galaxy Group (2PIGG) catalogue (Eke et al. 2004a).

By-products of this quest, which are also reported here, include a recalculation of the local galaxy near-infrared (near-IR) luminosity and stellar mass functions with the largest sample of galaxies yet used for this purpose. Mock galaxy catalogues are used in order to help quantify systematic uncertainties and biases. In addition, the dependence on group size of the stellar mass fraction and of the group mass-to-light and stellar mass-to-light ratios is studied and compared with previous results.

Section 2 contains a description of the data used in this analysis. The near-IR luminosity functions and mean luminosity densities are calculated in Section 3 and compared with recent determinations by Cole et al. (2001; hereafter C01), Kochanek et al. (2001) and Bell et al. (2003). Group total mass-to-light ratios in the K_S band are reported in Section 4. These results extend the range of group sizes over which near-IR mass-to-light ratios have been measured, relative to the studies of Kochanek et al. (2003), Lin, Mohr & Stanford (2003; hereafter LMS03) and Rines et al. (2004). Section 5 contains a description of the procedure used to calculate stellar masses given

⋆E-mail: v.r.eke@durham.ac.uk

a set of galaxy luminosities in different wavebands. The accuracy of these measurements is gauged using mock galaxy catalogues produced from a combination of a dark matter N-body simulation and a semi-analytical galaxy formation model. This information is then used in Section 6, where the total galaxy stellar mass function and $\Omega_{\rm stars}$ are estimated.

The stellar content of the galaxy population is split by group size in Section 7, where group stellar mass-to-light ratios and stellar mass fractions are presented and compared with those found by LMS03. Finally, Section 8 provides the constraint alluded to at the start of Section 1. Throughout this paper, it is assumed that $\Omega_{\rm m} = 0.3$, $\Omega_\Lambda = 0.7$ and the Hubble constant is written as $H_0 = 100\,h\,{\rm km\,s^{-1}\,Mpc^{-1}}$.

2 OBSERVATIONAL DATA

2.1 2dFGRS

The two contiguous patches of sky covered by the 2dFGRS contain approximately 190 000 galaxies with a median redshift of 0.11. For the purposes of the work performed in this paper, only the ∼109 000 galaxies at $z < 0.12$ were used. At higher redshifts, less than half of the $b_{\rm J}$-band luminosity of typical groups is contained within galaxies above the survey flux limit. The parent catalogue for the 2dFGRS has a very well quantified completeness. Norberg et al. (2002) and Cross et al. (2004) estimate that only ∼9 per cent of the $b_{\rm J}$-band luminosity is missing, while Driver et al. (2005) conclude from the Millennium Galaxy Catalogue (MGC) that the 2dFGRS-inferred luminosity density is ∼3 per cent low due to missing low surface brightness galaxies (at all luminosities).

In Sections 4, 7 and 8, where the galaxies are split by host group size, the 2PIGG catalogue (Eke et al. 2004a) has been used to define the galaxy groups and their properties. Note that in Section 8, where the distribution of stellar mass throughout the group population is studied, single galaxies are also defined as groups. While such groups do not have a dynamically estimated mass, they still have a well-defined total group luminosity.

2.2 2MASS

The near-IR data were obtained from the 2MASS XSC (Jarrett et al. 2000), using the data base available at http://irsa.ipac.caltech.edu/cgi-bin/Gator/nph-dd. A total of 43 553 $z < 0.28$ 2MASS galaxies were matched with those in the two contiguous patches of the 2dFGRS. The median redshift of the 2dFGRS galaxies with 2MASS matches is ∼0.095, slightly lower than the median of all 2dFGRS galaxies (∼0.11).

The total galaxy J-band magnitude was estimated from the J-band Kron measurement (corrected for galactic extinction), including an offset of −0.1 mag to account for flux outside the Kron aperture. This is approximate because of the variety of different surface brightness distributions among the galaxies, but it is a reasonable typical correction (C01). The total galaxy $K_{\rm S}$-band value is then inferred using the total J-band magnitude and the $J - K_{\rm S}$ colour within the 20 mag arcsec^{-2} isophotal fiducial elliptical aperture. Following C01, the $K_{\rm S}$-band Kron magnitudes (without the −0.1-mag shift) were compared with the deeper pointed observations of Loveday (2000). Fig. 1 shows that the 2MASS $K_{\rm S}$-band Kron values inferred from the J-band Kron magnitude and the isophotal colour are essentially unbiased, and have a scatter about the Loveday measurements, which depends strongly on magnitude. This represents an improvement over the first 2MASS data release used by C01, who needed to

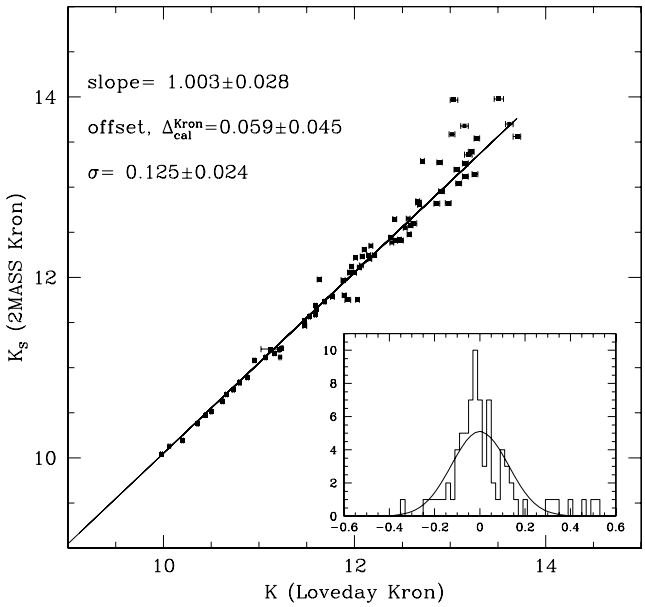

Figure 1. Comparison of the 2MASS K-band Kron magnitudes with those measured by Loveday (2000). A straight line traces the least-squares fit to the data. The inset histogram shows the distribution of magnitude differences between the 2MASS and Loveday measurements, which is interpreted as the distribution of errors in the 2MASS values. The best-fitting Gaussian is also shown, and its parameters are given in the legend.

apply an offset to match the Loveday data. For the whole sample of 80 galaxies, the distribution of errors, shown in the inset histogram, has a best-fitting Gaussian standard deviation of 0.125 mag.

When creating mock catalogues with near-IR galaxy magnitudes, it is necessary to include the observational errors in order to determine the systematic bias that they introduce. The medians of the binned errors on the J-band total magnitude and the $J - K_{\rm S}$ colour are shown in Fig. 2 as functions of the total J-band magnitude. These have been constructed using the 1σ uncertainties returned from the 2MASS data base. As was apparent in Fig. 1, the observational errors are greater for the fainter galaxies.

The $k + e$ corrections adopted for the J and $K_{\rm S}$ bands are

$$k + e = -\frac{(z + 4z^2)}{1 + 9z^{2.5}} \tag{2.1}$$

and

$$k + e = -\frac{(z + 15z^2)}{1 + 9z^{2.5}}, \tag{2.2}$$

respectively. These are fits to the mean of the $k + e$ corrections computed for individual galaxies using stellar population models. A detailed description of how the $k + e$ corrections are calculated can be found in C01. In brief, look-up tables of $b_{\rm J}$, $r_{\rm F}$, J and K magnitudes as a function of redshift were generated for a grid of star formation histories, using the stellar population spectral energy distributions provided by Bruzual & Charlot (2003). Observed galaxies were matched with theoretical star formation histories, thus allowing a $k + e$ correction to be assigned to each galaxy using the theoretical model. These simple models are used in Section 5 to assign stellar masses to galaxies.

Note that the mean $V/V_{\rm max} = 0.513$ for the 16 922 galaxies with $11.8 < J < 14.6$ and $z < 0.12$. In this expression, V represents the volume surveyed out to the redshift of each particular galaxy, and $V_{\rm max}$ is the maximum volume in which each galaxy could have been detected. The $K_{\rm S}$-band sample of 15 664 galaxies with

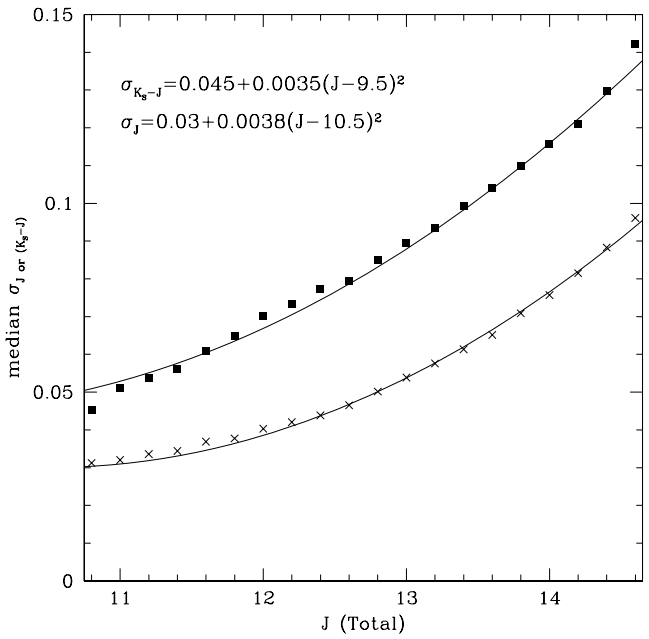

Figure 2. The errors on the 2MASS photometry are shown as functions of galaxy J-band total magnitude. Crosses and filled squares represent the medians of the J-band and $K_S - J$ 1σ uncertainties in each bin, i.e. the typical errors. The individual galaxy errors used to construct these medians are those contained in the 2MASS data base. The two lines trace the quadratic fits given in the panel.

$10.8 < K_S < 13.4$ and $z < 0.12$ has a mean $V(z_i)/V(z_{\max,i}) = 0.517$. These values suggest that the galaxy samples are not significantly incomplete (which would lead to values lower than 0.5) when these flux limits are applied. The top panels in Fig. 3 show the full distributions of $V(z_i)/V(z_{\max,i})$ for the samples used in the two bands, and the lower panels show the differential number counts

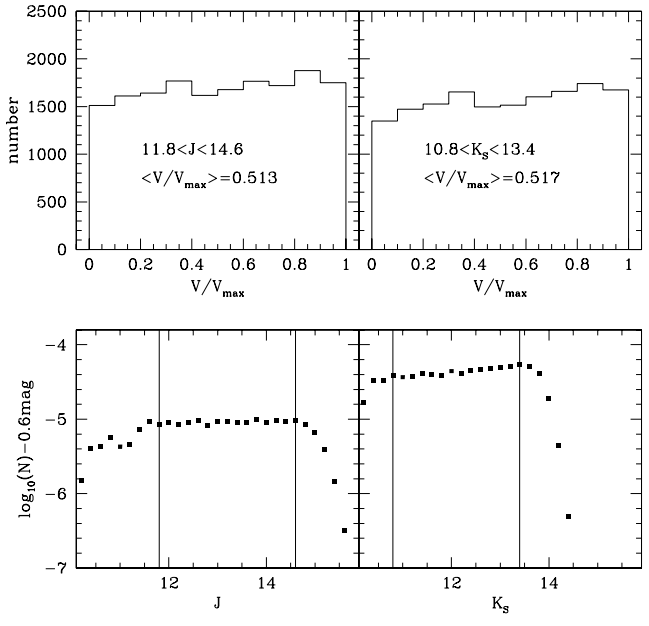

Figure 3. The top row shows the distributions of $V/V_{\max}$ for the J- (left) and K_S-band (right panel) samples. The lower row contains plots of the total number counts (N) as a function of magnitude for these same two bands. Vertical lines illustrate the flux limits applied to the survey in this paper.

with the Euclidean slope removed for all of the matched galaxies. These suggest that there is no strong systematic depletion of the galaxies near the adopted flux limits. Andreon (2002) and Bell et al. (2003) find a small incompleteness in the 2MASS survey arising from a deficit of faint, low surface brightness galaxies. While this makes a significant difference to the luminosity and stellar mass functions for the smaller galaxies, it has only a ∼20 per cent impact upon the total luminosity or stellar mass densities inferred from the data. This will be discussed further in Section 6.

3 LUMINOSITY FUNCTIONS

With the galaxy total J- and K_S-band magnitudes defined as described in the previous section, it is now possible to calculate the galaxy luminosity function in these bands. This analysis extends that by Kochanek et al. (2001) and C01, by using over twice as many galaxies, and also by adopting a different treatment of the statistical errors. In addition, mock 2dFGRS catalogues have been analysed to help determine the accuracy to which the luminosity functions can be recovered. The procedure for creating these mock catalogues was described in Eke et al. (2004a), and basically relies on populating dark matter haloes formed in the GIF N-body simulation (Jenkins et al. 1998) using the semi-analytical galaxy formation model described by Cole et al. (2000). In order to match the 2dFGRS b_J-band luminosity function, a luminosity-dependent colour-preserving shift is applied to each galaxy. However, the resulting model does not match the near-IR galaxy luminosity function. Thus, for the purposes of this paper, where the mock catalogue is being used to quantify errors in the recovered quantities rather than testing the galaxy formation model itself, an additional colour-preserving shift is applied when considering near-IR luminosities or stellar masses. In effect, each galaxy is made 15 per cent brighter, this being the factor necessary to increase the mean K_S-band luminosity density in the model to agree with that in the real data. This simulation cube filled with galaxies, hereafter referred to as the model, is then replicated and observed with suitable flux limits, masks, etc. (Norberg et al. 2002), creating a mock catalogue. While the mean K_S-band luminosity density is the same in mock and real catalogues, the luminosity function is not; so the near-IR flux limits applied to the mock catalogue are chosen to recover the same number of galaxies as are being considered from the 2MASS sample.

Figs 4 and 5 show the J- and K_S-band luminosity functions derived from both the mock catalogue and the 2dFGRS–2MASS data. Only the results obtained using a stepwise maximum likelihood estimator (SWML; Efstathiou, Ellis & Peterson 1988) are shown. A $1/V_{\max}$ estimator yields lower numbers of less luminous galaxies because both mock and real observers happen to live in underdense regions of universe. However, this estimator does give a reliable abundance at higher luminosities, where it probes a larger volume, and has thus been used to fix the normalization of the SWML curves. This was done using a χ^2 minimization in either of the intervals $10.1 < \log_{10}[L_J/(h^{-2}\,\mathrm{L}_\odot)] < 11.2$ or $10.4 < \log_{10}[L_{K_S}/(h^{-2}\,\mathrm{L}_\odot)] < 11.4$. Errors on the recovered SWML luminosity functions are determined from a jack-knife procedure. This entails splitting the galaxy sample, by right ascension, into 10 subsamples containing equal surveyed areas, recalculating 10 different estimates (n_i) of the luminosity function by rejecting each subsample in turn, then defining the uncertainty as

$$\sigma = \sqrt{\frac{10}{9}\sum_{i=1}^{10}(n_i - \bar{n})^2}, \qquad (3.1)$$

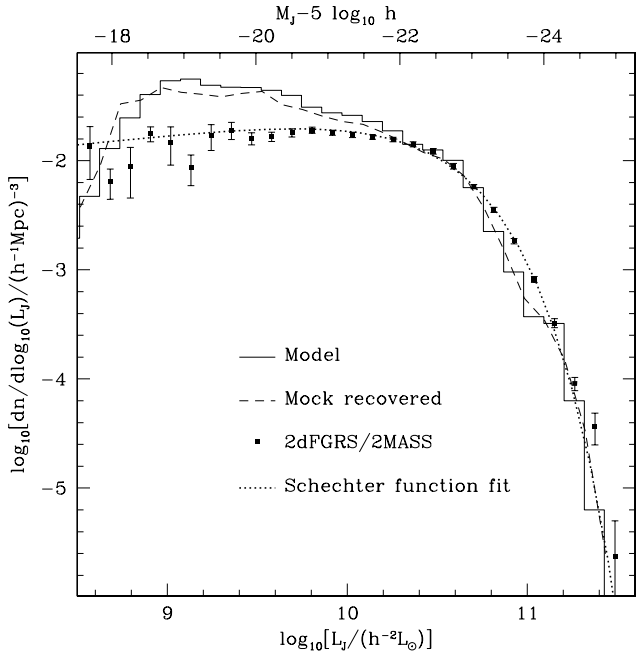

Figure 4. J-band luminosity functions for mock catalogues and 2dFGRS/2MASS data. The solid histogram traces the model galaxy J-band luminosity function, whereas the dashed line shows the luminosity function actually recovered from the mock catalogue using an SWML estimator, normalized to agree with the $1/V_{\rm max}$ luminosity function for $10.1 < \log_{10}[L_J/(h^{-2}\,{\rm L}_\odot)] < 11.2$. Results for the SWML estimate from the real data are shown with the points, and the error bars are inferred using a jack-knife method. The dotted line traces the best-fitting Schechter function derived from a χ^2 fit to the SWML estimate over the same range of luminosities used above. The Schechter function parameters are given in Table 1.

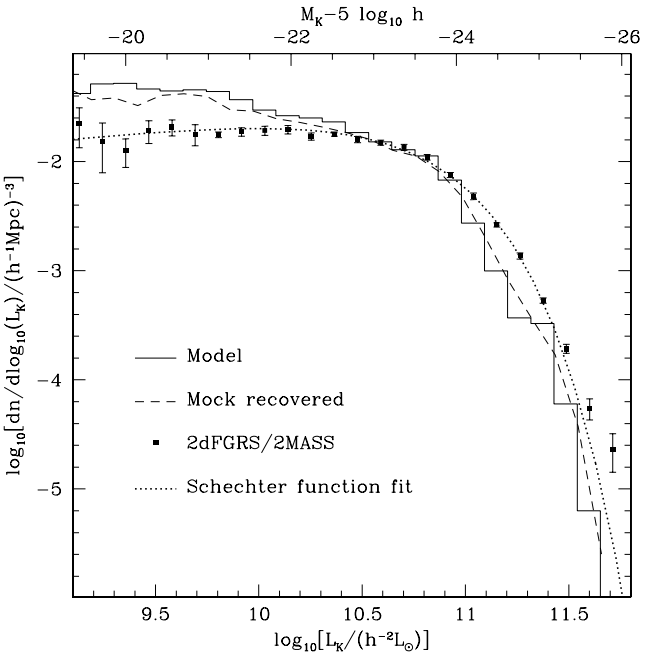

Figure 5. The equivalent of Fig. 4 for the $K_{\rm S}$-band luminosity functions. The SWML estimator has been normalized by matching to the $1/V_{\rm max}$ luminosity function at $10.4 < \log_{10}[L_{K_{\rm S}}/(h^{-2}\,{\rm L}_\odot)] < 11.4$.

where $(\bar{n})$ represents the luminosity function obtained using the full sample. The J and $K_{\rm S}$ luminosity functions estimated from the mock catalogue provide an accurate recovery of the underlying model function (shown with solid histograms), although they do differ somewhat from the near-IR luminosity functions estimated for the real data, despite having the same mean luminosity densities. The deficit of high-luminosity galaxies in the mock catalogue represents an interesting discrepancy between the semi-analytical model assumed in the mock catalogue and the real Universe.

Having normalized the SWML luminosity function using the luminous end of the $1/V_{\rm max}$ estimate, a χ^2 fit can be performed to determine the best-fitting Schechter (1976) function

$$\phi(L)\,{\rm d}L = \phi_* \left(\frac{L}{L_*}\right)^{\alpha} \exp\left(-\frac{L}{L_*}\right) \frac{{\rm d}L}{L_*}. \tag{3.2}$$

In principle, the range over which this fit is performed need not be restricted to the luminous galaxies. However, the impact of any potential low surface brightness incompleteness in 2MASS (Andreon 2002) is likely to be apparent at lower luminosities, so the fit is restricted to the same range of luminosities used to normalize the SWML function. Thus, the derived parameters, which are listed in Table 1, are also those that would have been found by fitting to the $1/V_{\rm max}$ estimate of the luminosity function.

The mean universal luminosity densities implied by the SWML-estimated luminosity functions are also included in Table 1. Statistical uncertainties come from the dispersion in the fits to the jack-knife samples. Note that, compared with the analysis of C01, the uncertainties on the luminosity function shape parameters (L_*, α) are larger, because of the limited range of luminosities over which the fit is performed. In contrast, the statistical uncertainty on the normalization is lower because of the increased sample size (both larger area and a deeper survey limit) and the choice of normalization method. Matching the abundance of high-luminosity galaxies is a better way of reducing the variance than fitting to the counts, as C01 did. Table 2 lists the SWML-estimated luminosity functions.

The statistical uncertainties are small compared to the systematic uncertainties. These include imperfections in the sample, due to incompleteness and misclassification in the parent 2dFGRS (Cross et al. 2004) and missing low surface brightness galaxies in the 2MASS (Andreon 2002; Bell et al. 2003). It is this last effect that is most important. Both Andreon (2002) and Bell et al. (2003) estimate that the 2MASS XSC misses ∼25 per cent of the mean luminosity density in the $K_{\rm S}$ band. The mean near-IR luminosity densities in Table 1 are consistent with those of C01 and Bell et al. (2003), but have smaller statistical uncertainty.

4 $K_{\rm S}$-BAND GROUP MASS-TO-LIGHT RATIOS

Following Eke et al. (2004b), who studied the $b_{\rm J}$- and $r_{\rm F}$-band galactic content of groups of different size, the near-IR group mass-to-light ratio (Υ_K) is now considered. As the total galaxy stellar mass correlates more strongly with the near-IR flux than it does with the optical flux, Υ_K more effectively reflects the efficiency with which stars have been formed in regions that end up in these different-sized haloes.

4.1 Results for the model

Fig. 6 shows how the star formation efficiency varies with halo size. The model used to populate the mock catalogues shows a clear minimum in mass-to-light ratio at group sizes corresponding to about one L_* galaxy, as was seen in the optical bands (Eke et al. 2004b),

Table 1. Best-fitting Schechter function parameters for the different galaxy luminosity functions. The normalizations come from a χ^2 fit to the $1/V_{\rm max}$ estimate of the abundances of the most luminous galaxies. Also listed are the adopted solar absolute magnitudes in the two bands and the mean universal luminosity densities implied by the SWML functions. Only statistical uncertainties are quoted. The larger systematic uncertainties are discussed in the text. No account has been taken of the systematic impact of the errors in the 2MASS magnitudes. However, this effect is smaller than the quoted statistical uncertainties.

Band	M_*	$L_*/(h^{-2}\,{\rm L}_\odot)$	α	$\phi_*/(h^{-1}\,{\rm Mpc})^{-3}$	$\rm M_\odot$	$\bar\rho/(h\,{\rm L}_\odot\,{\rm Mpc}^{-3})$
J	-22.39 ± 0.05	$(2.81 \pm 0.12) \times 10^{10}$	-0.82 ± 0.06	$(1.39 \pm 0.06) \times 10^{-2}$	3.73	$(3.57 \pm 0.11) \times 10^8$
$K_{\rm S}$	-23.43 ± 0.04	$(5.36 \pm 0.22) \times 10^{10}$	-0.81 ± 0.07	$(1.43 \pm 0.08) \times 10^{-2}$	3.39	$(7.04 \pm 0.23) \times 10^8$

Table 2. The near-IR luminosity functions recovered with the real data. Luminosities are measured in $h^{-2}\,{\rm L}_\odot$ and the quoted abundances are ${\rm d}n/{\rm d}\log_{10}L$ in $(h^{-1}\,{\rm Mpc})^{-3}$.

$\log_{10}(L)$	J band	$K_{\rm S}$ band
8.50	$(1.08 \pm 0.60) \times 10^{-2}$	
8.62	$(1.06 \pm 0.45) \times 10^{-2}$	
8.74	$(5.70 \pm 2.82) \times 10^{-3}$	
8.86	$(1.41 \pm 0.32) \times 10^{-2}$	
8.98	$(1.65 \pm 0.47) \times 10^{-2}$	
9.10	$(8.70 \pm 3.30) \times 10^{-3}$	$(1.62 \pm 0.63) \times 10^{-2}$
9.22	$(1.44 \pm 0.39) \times 10^{-2}$	$(1.71 \pm 0.80) \times 10^{-2}$
9.34	$(1.85 \pm 0.35) \times 10^{-2}$	$(1.14 \pm 0.37) \times 10^{-2}$
9.46	$(1.55 \pm 0.20) \times 10^{-2}$	$(1.79 \pm 0.43) \times 10^{-2}$
9.58	$(1.60 \pm 0.16) \times 10^{-2}$	$(1.97 \pm 0.33) \times 10^{-2}$
9.70	$(1.74 \pm 0.15) \times 10^{-2}$	$(1.69 \pm 0.36) \times 10^{-2}$
9.82	$(1.83 \pm 0.11) \times 10^{-2}$	$(1.70 \pm 0.09) \times 10^{-2}$
9.94	$(1.71 \pm 0.09) \times 10^{-2}$	$(1.80 \pm 0.17) \times 10^{-2}$
10.06	$(1.64 \pm 0.09) \times 10^{-2}$	$(1.87 \pm 0.17) \times 10^{-2}$
10.18	$(1.56 \pm 0.07) \times 10^{-2}$	$(1.79 \pm 0.16) \times 10^{-2}$
10.30	$(1.45 \pm 0.07) \times 10^{-2}$	$(1.64 \pm 0.10) \times 10^{-2}$
10.42	$(1.28 \pm 0.07) \times 10^{-2}$	$(1.64 \pm 0.09) \times 10^{-2}$
10.54	$(1.01 \pm 0.06) \times 10^{-2}$	$(1.46 \pm 0.09) \times 10^{-2}$
10.66	$(6.62 \pm 0.33) \times 10^{-3}$	$(1.36 \pm 0.08) \times 10^{-2}$
10.78	$(4.02 \pm 0.19) \times 10^{-3}$	$(1.14 \pm 0.07) \times 10^{-2}$
10.90	$(2.11 \pm 0.12) \times 10^{-3}$	$(7.97 \pm 0.41) \times 10^{-3}$
11.02	$(9.11 \pm 0.55) \times 10^{-4}$	$(4.99 \pm 0.33) \times 10^{-3}$
11.14	$(3.49 \pm 0.32) \times 10^{-4}$	$(2.69 \pm 0.13) \times 10^{-3}$
11.26	$(9.17 \pm 1.23) \times 10^{-5}$	$(1.34 \pm 0.09) \times 10^{-3}$
11.38		$(4.90 \pm 0.27) \times 10^{-4}$
11.50		$(1.66 \pm 0.17) \times 10^{-4}$
11.62		$(4.24 \pm 1.08) \times 10^{-5}$
11.74		$(1.68 \pm 0.66) \times 10^{-5}$

as well as a plateau for clusters with $\log_{10}(L_{b_{\rm J}}/h^{-2}\,{\rm L}_\odot) > 11.5$. The process of identifying groups and inferring their mass-to-light ratios using a dynamical mass estimator inevitably introduces errors. A dotted line traces the mass-to-light ratio variation recovered from the mock catalogue. In selecting the groups to be used to make this curve, only local and isolated ones are taken, to avoid some sources of contamination. As a consequence of these restrictions, which are detailed in the caption of Fig. 6, the group mass-to-light ratio can be recovered to within ∼50 per cent for groups with $\log_{10}(L_{b_{\rm J}}/h^{-2}\,{\rm L}_\odot) > 10.5$. The main source of bias is due to interloping galaxies in the groups, which tend to increase the luminosity more than the mass (the groups are found in redshift space, so interlopers have velocities similar to those of true group members). An increase of Υ_K by a factor of 3 in going from $\log_{10}(L_{b_{\rm J}}/h^{-2}\,{\rm L}_\odot) = 10.5$ to 11.3 is recovered, which is comparable to that present in the model haloes, albeit shifted to slightly larger halo luminosity.

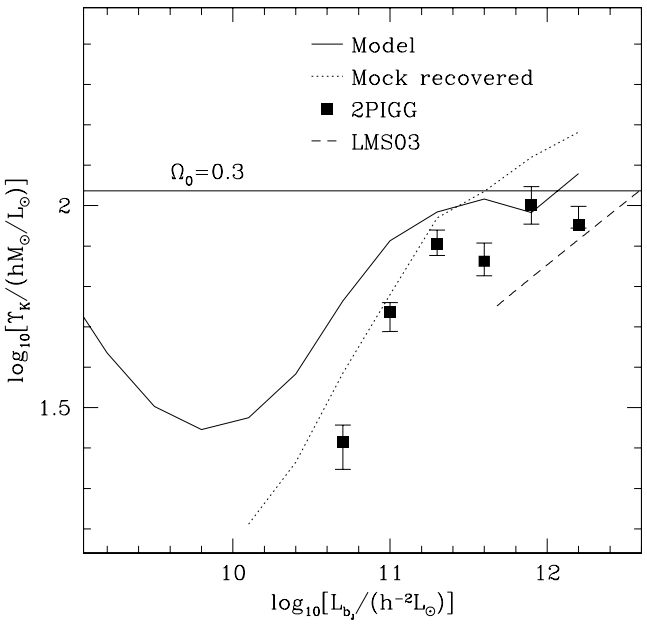

Figure 6. The variation of the mock and 2PIGG $K_{\rm S}$-band mass-to-light ratios with halo size, parametrized by the total $b_{\rm J}$-band luminosity contained in the halo. A horizontal line shows the mean mass-to-light ratio of the model, while the solid curve traces the variation of the binned median mass-to-light ratio in the model. The accuracy with which this is recovered is shown by the dotted line, and the points display the results obtained from the real 2PIGG sample. Only groups with no neighbours within a distance of $d_{\rm min}/h^{-1}\,{\rm Mpc} = 2 + [10 - \log_{10}(L_{b_{\rm J}}/h^{-2}\,{\rm L}_\odot)]$ and out to a maximum redshift of $z_{\rm max} = 0.04 + 0.03\,[\log_{10}(L_{b_{\rm J}}/h^{-2}\,{\rm L}_\odot) - 10]$ are considered. Error bars show the 16th and 84th percentiles in each bin. A dashed line traces the results of Lin, Mohr & Stanford (2003), mapped on to these axes using the median mass-to-$b_{\rm J}$ light found by Eke et al. (2004b), and assuming that the clusters have a concentration of 5. Taking the median group total mass-to-light ratio of Eke et al. (2004b) maps the following luminosities $\log_{10}[L_{b_{\rm J}}/(h^{-2}\,{\rm L}_\odot)] = (10, 11, 12)$ to masses $\log_{10}[{\rm M}_\odot/(h^{-1}\,{\rm M}_\odot)] = (12.0, 13.6, 14.7)$.

4.2 Observational data

The points in Fig. 6 represent the result of applying the same group-finding, mass-to-light ratio measuring and group-selecting procedure to the 2dFGRS as was applied to the mock catalogue. Again, a factor of ∼3 increase in Υ is visible when going from the smaller groups to rich clusters. All of this trend occurs at $\log_{10}(L_{b_{\rm J}}/h^{-2}\,{\rm L}_\odot) < 11.3$. Above $\log_{10}(L_{b_{\rm J}}/h^{-2}\,{\rm L}_\odot) \approx 11.3$, the near-IR group mass-to-light ratio remains approximately constant. This higher luminosity range corresponds to the range of cluster sizes in the sample of Lin et al. (2003, LMS03). They find that the $K_{\rm S}$-band $\Upsilon_{500} \propto M_{500}^{0.31\pm0.09}$. This slope is steeper than suggested by the data presented here, which are in better agreement

with the results of Kochanek et al. (2003). They find this exponent to be 0.10 ± 0.09, despite going down to smaller groups [$\log_{10}(L_{b_J}/h^{-2}\,\mathrm{L}_\odot) \approx 10.8$], where the trend starts to become apparent in the 2PIGG results.

For the 110 groups with $\log_{10}(L_{b_J}/h^{-2}\,\mathrm{L}_\odot) \geqslant 11.3$, the median $\Upsilon_K = 89 \pm 3\,h\Upsilon_\odot$ (statistical uncertainty only). If the 2PIGG mass-to-light ratios for such clusters are overestimated by the same factor as in the mock catalogues, then one should correct the median mass-to-light ratio downwards accordingly to yield $\Upsilon_K = 77 \pm 3\,h\Upsilon_\odot$. This is very similar to the value found by LMS03. For a sample of 19 clusters with $kT_\mathrm{X} \geqslant 3.7$ keV, they obtained $\Upsilon_K = 76 \pm 4\,h\Upsilon_\odot$ using the 2MASS K_S-band group luminosities with a statistical background correction, and masses inferred from X-ray data and the assumption of hydrostatic equilibrium. The LMS03 clusters extend to blue luminosities of $\log_{10}(L_{b_J}/h^{-2}\,\mathrm{L}_\odot) \sim 13$, off the right hand side of Fig. 6, and it is these higher luminosity clusters that bring the median mass-to-light ratio up into agreement with the 2PIGG results. Kochanek et al. (2003) find $\Upsilon_K = 116 \pm 46\,h\Upsilon_\odot$, which is consistent within the statistical uncertainty.

There are a number of potential systematic differences that blur the comparison between the cluster K_S-band mass-to-light ratios reported in different papers, at a level of ∼10 per cent. These include the possibility of galaxies not tracing dark matter in real haloes as they do in the model universe and incompleteness in the parent 2dFGRS. The LMS03 value is measured at a radius, r_{500}, enclosing a mean density of 500 times the critical value, whereas the group definition used here is tuned to the halo found by applying a friends-of-friends group-finder, with a linking length equal to 0.2 times the mean interparticle separation, to a dark matter simulation. This algorithm finds groups out to a radius $r_\mathrm{vir} \approx r_{200} > r_{500}$. Rines et al. (2004) find that the variation of mass-to-light ratio with radius is slight in their sample of nine rich clusters. They use mass profiles determined from the infall pattern of galaxies. Combining this with an assumption that the dark matter haloes have Navarro, Frenk & White (NFW, 1997) profiles with a concentration of 5, they find that the mean mass-to-light ratios are $\Upsilon(<r_{500}) = 78 \pm 7\,h\Upsilon_\odot$ and $\Upsilon(<r_{200}) = 88 \pm 9\,h\Upsilon_\odot$.

4.3 Estimating Ω_m

Given the K_S-band mass-to-light ratio of clusters, an assumption as to how this compares to the mean universal mass-to-light ratio and a measurement of the mean luminosity density, yields an estimate of Ω_m. If real clusters, like the model clusters, have mass-to-light ratios that underestimate the mean universal value, then this exercise gives $\Omega_\mathrm{m} = 0.21 \pm 0.01$ (statistical). This value is obtained after applying two largely offsetting ∼10 per cent corrections, one assuming that the cluster mass-to-light ratio is overestimated and the other that it provides an underestimate of the universal value, so the statistical error is likely to bear little relation to the true uncertainty on this estimate. It is interesting to note that this estimate of Ω_m is somewhat lower than that produced by Eke et al. (2004b) using a similar method in the b_J and r_F bands ($\Omega_\mathrm{m} \approx 0.27$).

While the total K_S-band luminosity density in the mock is the same as that in the real world, the mock clusters have mass-to-light ratios that are ∼30 per cent greater than those in the real world. If the mock catalogues had more faithfully represented the real shape of the K_S-band galaxy population, then not only would more luminous galaxies have existed in the model but, perhaps, they would have preferentially occurred in rich clusters. The net effect would have been to make the cluster mass-to-light ratio a smaller fraction of the universal mean. Consequently, a larger correction upwards would have been required, and when applied to the real data a higher Ω_m would have resulted. Given the systematic differences between the mock catalogue and the real data in the K_S band, it would be premature to say that this low apparent value of Ω_m represents anything more than a challenge for semi-analytical models to place more K_S-band luminosity into clusters.

5 STELLAR MASS ESTIMATES

The stellar mass of a galaxy can be estimated from its redshift and broad-band magnitudes using simple stellar population synthesis models. Two different sets of models are employed here, characterized by ranges of metallicity and exponential time-scales for the assumed star formation, with the additional possibility of a separate burst of star formation. The first choice is very similar to that described at length by C01. In summary, a grid of star formation histories is constructed, in which both the e-folding time, τ, which governs the star formation rate [$\psi \propto \exp(-t/\tau)$] and the metallicity, Z, of the stars are varied. The allowed ranges are $1 \leqslant \tau/\mathrm{Gyr} \leqslant 100$ and $10^{-4} \leqslant Z \leqslant 0.05$. When combined with the assumption of a Kennicutt (1983) stellar initial mass function (IMF) and the stellar population synthesis models of Bruzual & Charlot (2003), look-up tables of broad-band magnitudes versus redshift can be generated. Each observed set of galaxy magnitudes is matched with the theoretical model that best reproduces these magnitudes at the redshift of the galaxy. The theoretical track can then be used to estimate the $k + e$ correction that should be applied to calculate the absolute magnitude of the galaxy (see Section 2.2), and also to infer its mass-to-light ratio at $z = 0$. There are two major differences between the stellar masses computed here and those inferred by C01. First r_F magnitudes have now been measured for the 2dFGRS objects. Secondly, models are selected from a sparser theoretical grid to produce unique predictions for colour versus redshift, whereas the tracks used by C01 sampled e-folding time and metallicity so finely that more than one choice could give rise to a galaxy of the same colour.

With the availability of r_F magnitudes, there is now more information to help assess which theoretical model best matches the colours of each observed galaxy. Throughout the rest of this paper, two different stellar mass estimators will be referred to. The J-band stellar mass will be that coming from using all four fluxes (b_J, r_F, J and K_S) to choose a model star formation history. The second estimate, the r_F-band-inferred stellar mass, will be identical to the J-band estimate when near-IR fluxes are available, but will also include galaxies too faint to make the near-IR flux limit of the sample. In these cases, the r_F-inferred mass will be based on just the b_J and r_F data. These two stellar mass estimates should thus be considered to represent two different subsets of galaxies, with the r_F-inferred stellar masses providing a deeper sample that reaches higher redshifts and intrinsically less massive galaxies than the J-band sample.

Note that the choice of stellar IMF introduces a large systematic uncertainty in the recovered stellar masses. For instance, as C01 showed, a Salpeter IMF assigns almost twice as much stellar mass per unit light as is inferred using the Kennicutt IMF, which is used throughout this paper. It should also be stressed that the stellar masses referred to in this paper are those currently locked up in stars. This differs from the total mass of star formation by a factor that depends on how much stellar mass is recycled. Following Cole et al. (2000), a recycled fraction of $R = 0.42$ is adopted throughout this paper to approximate this effect for a Kennicutt IMF.

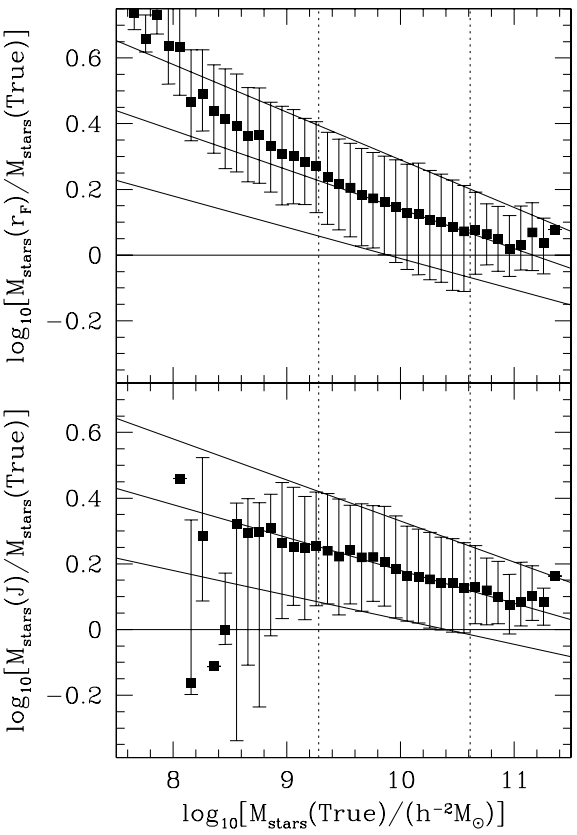

Figure 7. Errors in the inferred stellar masses using the $r_{\rm F}$- (upper panel) and J-band (lower panel) estimators. The points show the median binned accuracy with which stellar masses are recovered from the mock catalogue using the $r_{\rm F}$-band stellar masses. Error bars display the 16th and 84th percentiles. All galaxies at $z < 0.12$ have been used to calculate these quantities. The solid lines represent fits to the median ± 34 percentiles given in equations (5.1)–(5.3). Dotted vertical lines delimit the region containing the central 80 per cent of the stellar mass (i.e. only 10 per cent comes from each region outside the dotted lines).

Another uncertainty in the estimated stellar masses is the appropriateness of the assumed exponential star formation history. It is possible, however, to estimate the size of this error using the mock catalogues. Fig. 7 shows how well the recovery works for the $r_{\rm F}$- and J-band stellar masses referred to above, as a function of the true stellar mass in the model galaxy. The inclusion of magnitude errors contributes little to the range of stellar mass errors, which are instead dominated by the choice of the grid of star formation histories. While the grid of models assumes that the stars formed with a single exponential time-scale, the more realistic semi-analytical galaxies undergo much more complex, bursty histories. Consequently, some non-negligible error in the estimated stellar masses is to be expected. As shown in Fig. 7, the recovered stellar masses are systematically too high by a few tens of per cent. Rough fits to the typical errors in the stellar mass recovery and the scatter about this error are shown with the lines in Fig. 7. The equations of these lines are, for the $r_{\rm F}$ band,

$$y = 1.34 - 0.12x \tag{5.1}$$

and

$$\sigma_y = 0.4 - 0.025x, \tag{5.2}$$

where $y = \log_{10}[M_{\rm stars}({\rm estimated})/M_{\rm stars}({\rm true})]$ and $x = \log_{10}[M_{\rm stars}({\rm true})/(h^{-2}\,{\rm M}_\odot)]$, and for the J band

$$y = 1.18 - 0.10x \tag{5.3}$$

and the same σ_y as above. This discrepancy is of a similar size to the systematic differences between the various stellar mass estimates used by Drory, Bender & Hopp (2004). They find a trend, whereby lower mass galaxies have photometrically inferred stellar masses that increasingly overestimate the dynamically inferred masses. In contrast to their study, where they cannot tell which stellar mass estimator is the best, the true stellar masses are known for the galaxies in the mock catalogues used here. Thus, it is possible either to calibrate the bias, or to improve the set of model tracks that are used to fit the galaxy colours. The second option has been taken, and a second grid of star formation histories has been introduced in an attempt to reduce the bias in the estimated stellar masses.

As the overestimation of the stellar masses had been driven by the fitted model trying to match the blueness of the observed galaxies by artificially decreasing the metallicity and increasing the star formation time-scale, an additional 5 per cent (by mass) burst of star formation was introduced into the new model tracks to help fit the colours of the bluest galaxies. This single burst can occur at a finite set of times throughout the evolution of the galaxy. Constraining the metallicity to be $Z = 0.005$ and leaving the set of time-scales, τ, to be as before led to the results shown in Fig. 8. Note how the results have improved such that the median recovered stellar masses are now almost unbiased for the bulk of the $r_{\rm F}$-band stellar mass. The J-band stellar mass estimates are improved, but still biased slightly high, as shown by the fit given by $y = 0.1$ and the same σ_y as above. This new set of model tracks provides a significantly more accurate set of stellar mass estimates than the previously adopted ones.

6 THE TOTAL STELLAR MASS FUNCTION

For each of the stellar mass estimates, it is possible to determine the total stellar mass function in galaxies. The mock catalogues provide guidance on the size of possible systematic errors arising from the measurement procedure. Both $1/V_{\rm max}$ and bivariate SWML (Sodré & Lahav 1993; Loveday 2000) methods have been employed. The former method is sensitive to large-scale fluctuations in the galaxy density field, and is thus less reliable for the low stellar masses that are only seen locally. However, the high-mass end with $10.4 \leqslant \log_{10}(M_{\rm stars}/\,h^{-2}\,{\rm M}_\odot) \leqslant 11.4$ provides a good normalization of the SWML method, which is insensitive to these density fluctuations, but only returns a shape for the stellar mass function. A bivariate SWML method is necessary, with the variables being the inferred stellar mass and the galaxy luminosity in the waveband defining the survey (i.e. $b_{\rm J}$ or J for the $r_{\rm F}$- and J-band stellar masses, respectively).

6.1 Systematic errors in the recovery

Fig. 9 shows how well the stellar mass function can be recovered from the mock catalogue. Only galaxies with $z < 0.12$ are used in constructing these functions. It is apparent that the effect of the measurement errors in the galaxy J-band stellar masses is to produce an overestimate of the abundance of galaxies at the higher stellar masses. This, in turn, is reflected in an overestimation of the contribution to the cosmic density from stars residing in galaxies. While the model value is $\Omega_{\rm stars}h = 1.12 \times 10^{-3}$ (from integrating under the solid black line multiplied by $M_{\rm stars}$), and the fraction of universe that is actually probed by the mock survey only has

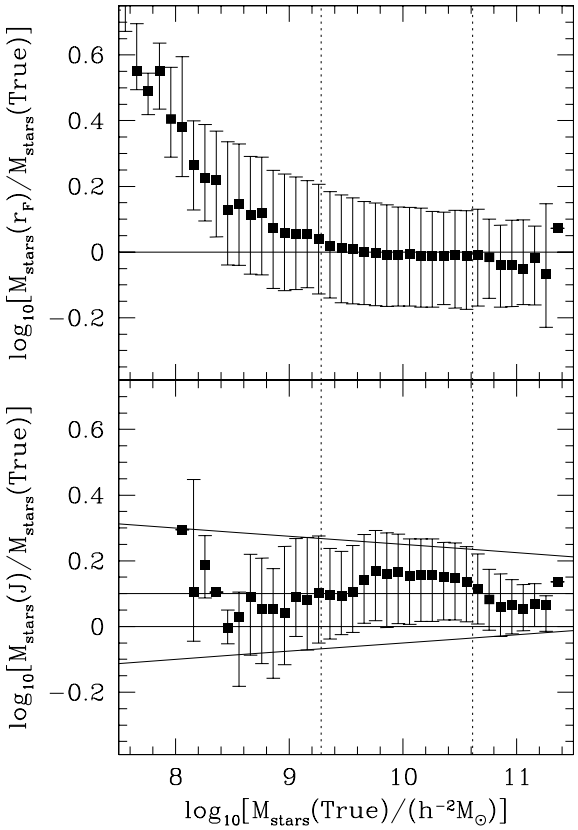

Figure 8. Errors in the inferred stellar masses using the new $r_{\rm F}$- (upper panel) and J-band (lower panel) estimators, incorporating bursts. The points show the median binned accuracy with which stellar masses are recovered from the mock catalogue using the $r_{\rm F}$-band stellar masses. Error bars display the 16th and 84th percentiles. All galaxies at $z < 0.12$ have been used to calculate these quantities. The extra solid lines in the lower panel represent fits to the median ± 34 percentiles. Dotted vertical lines delimit the region containing the central 80 per cent of the stellar mass (i.e. only 10 per cent comes from both regions not between dotted lines).

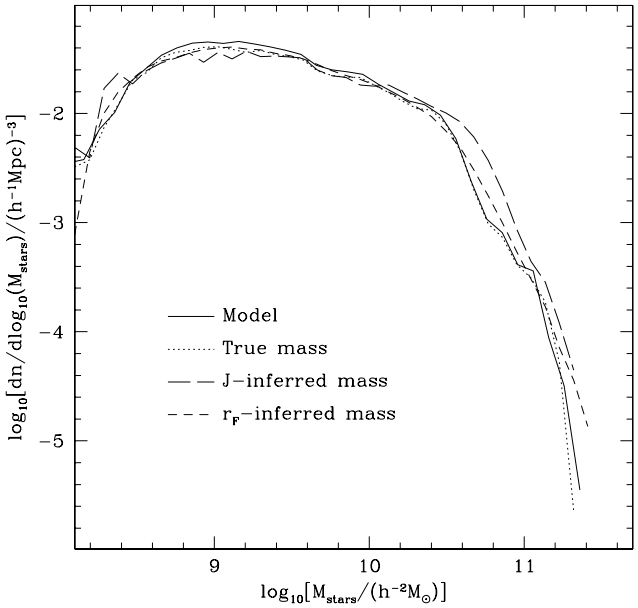

Figure 9. Systematic errors in the recovery of the global stellar mass function. The solid line traces the stellar mass function in the model. The dotted line shows an SWML estimate of the stellar mass function from the mock catalogue using the true stellar masses, rather than those inferred from the galaxy light. Long- and short-dashed lines trace the normalized SWML stellar mass functions estimated from the mock, using the J- and $r_{\rm F}$-band-inferred stellar masses. The abundance drops for galaxies with $\log_{10}(M_{\rm stars}/\,h^{-2}\,{\rm M}_{\odot}) \lesssim 9$ because of the blue luminosity limit in the model galaxy population, $M_{b_{\rm J}} \leqslant -16$.

$\Omega_{\rm stars}h = 1.02 \times 10^{-3}$ (dotted line) because of variations due to large-scale structure, the recovered SWML values are $\Omega_{\rm stars}h = 1.06 \times 10^{-3}$ (short-dashed line) and $\Omega_{\rm stars}h = 1.29 \times 10^{-3}$ (long-dashed line) for the $r_{\rm F}$- and J-band measurements, respectively. To give an idea of the size of the error that can be introduced by using the $1/V_{\rm max}$ stellar mass function, rather than the suitably normalized SWML one, the J-band $1/V_{\rm max}$ stellar mass function yields a value of $\Omega_{\rm stars}h = 1.13 \times 10^{-3}$, $\sim$15 per cent down on the SWML estimate, which is unaffected by the large-scale density fluctuations.

Fig. 10 shows the stellar mass function obtained by convolving the model with a Gaussian whose mean and width vary with stellar mass according to the lines in the lower panel of Fig. 8. The fact that this matches very well the stellar mass function inferred from the J-band mock catalogue demonstrates that this is the uncertainty that causes the systematic bias in the recovery of the stellar mass function. Performing this experiment using the original set of model tracks to infer stellar masses leads to an overestimate of $\Omega_{\rm stars}h$ by $\sim$40 per cent, for both the $r_{\rm F}$- and J-band stellar mass cases. While the size of this error is merely comparable with the systematic uncertainty arising from the choice of stellar IMF, it is larger than the statistical uncertainties quoted by C01 and Bell et al. (2003), and should be corrected for. Note that Bell et al. use a different procedure to calculate stellar masses, so the bias introduced by their method may not be quite the same as that found in this work.

From the mock catalogue, it is apparent that an SWML estimator of the stellar mass function is preferable to $1/V_{\rm max}$, and that the uncertainties in the stellar mass estimation lead to a bias in the inferred value of $\Omega_{\rm stars}h$. However, the new model tracks are such that this bias is negligible for the $r_{\rm F}$-inferred stellar masses and only $\sim$25 per cent for the J-band case. Given that this overestimation results largely from the method chosen to assign stellar masses, it seems likely that such a systematic error would also be present when this technique is applied to real data. In subsequent sections, the real data will sometimes be 'corrected', under the assumption that the same bias exists in results from both mock and real catalogues.

6.2 Comparison with other studies

Applying the $1/V_{\rm max}$ and SWML estimators to the full 2dFGRS–2MASS sample within $z = 0.12$ yields the results shown in Fig. 11. Comparing with the results of C01, who used both Kennicutt (1983) and Salpeter (1955) IMFs, it is apparent that the new J-band results are similar at higher stellar masses. For the smaller systems, the J-band mass function, which should be comparable with that of C01, apart from the different set of model tracks being used to infer stellar masses, shows a deficit. The $r_{\rm F}$-band function does include most of the low stellar mass systems found by C01. Note that the stellar masses of the best-fitting Schechter function of C01 have been multiplied by 1.1 to take into account, roughly, the difference between Kron and total magnitudes. The discrepancy with C01 is mainly for the low-mass galaxies, and thus does not greatly impact upon the inferred value of $\Omega_{\rm stars}h$. Assuming a Kennicutt IMF, C01

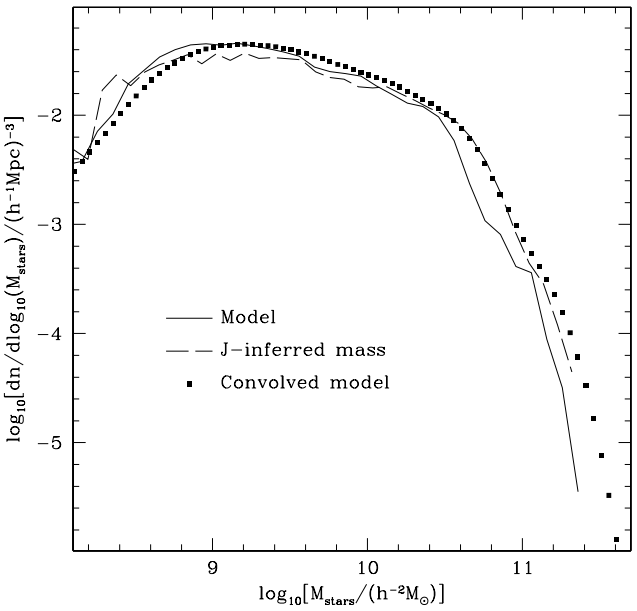

Figure 10. How stellar mass uncertainties affect the estimated stellar mass function. The solid line traces the stellar mass function in the model. The dashed line shows the SWML estimate of the stellar mass function from the mock catalogue using the *J*-band stellar masses. Points show the effect of convolving the model stellar mass function with a mass-dependent Gaussian, of mean and width given by the straight lines in Fig. 8.

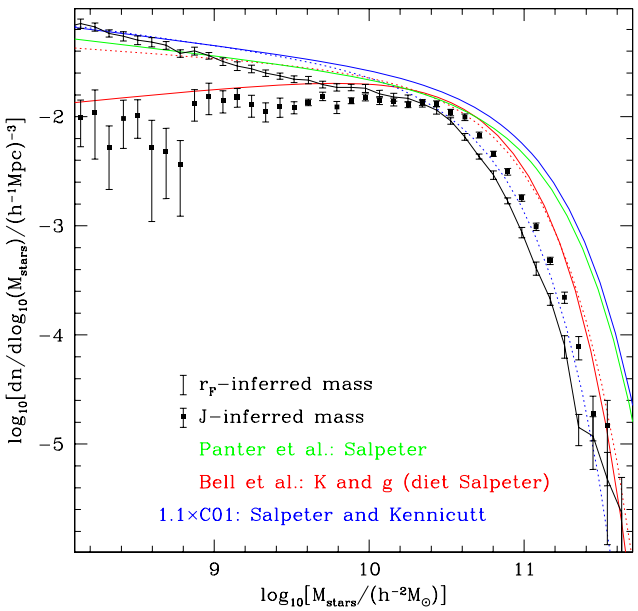

Figure 11. The uncorrected stellar mass functions calculated using the real 2dFGRS–2MASS sample of galaxies. This figure is colour in the online version of the article. SWML results from both *J*- (filled squares) and $r_{\rm F}$-band (black line with errors) stellar mass estimators are shown. Also shown are the best-fitting Schechter functions advocated by Panter, Heavens & Jimenez (Salpeter IMF; green); C01 (Salpeter; solid blue); C01 (Kennicutt; dotted blue) and Bell et al. – *K* band (solid red) and *g* band (dotted red).

found $\Omega_{\rm stars}h = (1.6 \pm 0.24) \times 10^{-3}$, whereas the corresponding numbers found here are $(1.23 \pm 0.01) \times 10^{-3}$ and $(1.32 \pm 0.06) \times 10^{-3}$ for the $r_{\rm F}$ and *J* band, respectively. As described above, it is entirely conceivable that these, already lower, estimates of $\Omega_{\rm stars}h$ are nevertheless still overestimated as a result of the errors inherent in assigning stellar masses to galaxies. Correcting these estimates under the assumption that they suffer the same fractional overestimates as the mock data gives the corrected $\Omega_{\rm stars}h$ values in the final column of Table 3. Also listed in Table 3 are the best-fitting Schechter function parameters obtained by a χ^2 fit to the normalized SWML stellar mass functions (see Table 4) over the range $9.5 \leqslant \log_{10}(M_{\rm stars}/h^{-2}\,{\rm M}_\odot) \leqslant 11.4$ for the $r_{\rm F}$-band stellar masses and $10.0 \leqslant \log_{10}(M_{\rm stars}/h^{-2}\,{\rm M}_\odot) \leqslant 11.4$ for the *J*-band stellar masses. The quoted statistical uncertainties are estimated from the scatter in the fits to the jack-knife subsamples. In addition to the systematic uncertainties in the luminosity function estimation, a further source of systematic uncertainty is the poorly known stellar IMF. To give a rough idea of how large an effect this can have, C01 find that a Salpeter IMF yields a mean stellar mass density that is almost twice as large as that implied by the Kennicutt IMF.

The difference between the stellar mass functions inferred using the two different mass estimators is consistent with what was found by Bell et al., namely, that the sample selected by 2MASS flux is incomplete as a result of missing low surface brightness galaxies. This was shown by Bell et al. comparing a 2MASS *K*-selected sample with a Sloan Digital Sky Survey (SDSS) *g*-band one. Their results exhibit a deficit of 2MASS-selected galaxies at $\log_{10}[M_{\rm stars}/(h^{-2}\,{\rm M}_\odot)] < 10$, very similar to the mass at which the *J*- and $r_{\rm F}$-band results found here begin to differ.

Combining the estimate of the mean stellar density and the luminosity density from the previous section yields an estimate of the mean stellar mass-to-light ratio. Taking the average of the uncorrected $\Omega_{\rm stars}(r_{\rm F})$ and $\Omega_{\rm stars}(J)$ values, because it is unclear which is better, gives a mean $K_{\rm S}$-band stellar mass-to-light ratio of $0.5\Upsilon_\odot$. If the corrected stellar mass densities are employed instead, then this reduces to $0.44\Upsilon_\odot$. Even the uncorrected value is ∼30 per cent lower than that found by C01 ($0.73 \pm 0.15\Upsilon_\odot$).

7 STELLAR MASSES IN DIFFERENT-SIZED GROUPS

The 2PIGG catalogue allows a detailed study of how the galaxy stellar mass is distributed among groups of different size. This section presents measurements of the stellar mass-to-light ratio and the stellar mass fraction, both as functions of group size.

When calculating total group stellar masses, it is necessary to include the contributions by group members that do not make it into the flux-limited sample. This is done through the global bivariate SWML distribution of stellar mass and galaxy luminosity. Integrating this distribution over all stellar masses gives the fraction of stellar mass above a particular galaxy luminosity. The reciprocal of this fraction is the factor by which the total observed stellar mass must be increased in order to obtain the total group stellar mass.

7.1 Group stellar mass-to-light ratios

The stellar mass-to-light ratio in the $K_{\rm S}$ band is shown as a function of total group $b_{\rm J}$ luminosity in Fig. 12. Only groups with $z < z_{\rm max} = 0.05 + 0.02[\log_{10}(L_{b_{\rm J}}/h^{-2}\,{\rm L}_\odot) - 10]$ are used, this being an appropriate compromise between having enough groups, and being able to see most of their stellar mass and luminosity. It is apparent that the values recovered from the mock generally overestimate the model mass-to-light ratio for the *J*-inferred stellar masses. This can be traced directly to the results shown in Fig. 8. The $r_{\rm F}$-band stellar masses tend to recover an underestimated stellar

Table 3. Best-fitting Schechter function parameters for the different galaxy SWML stellar mass functions. The SWML estimates are normalized using a χ^2 fit to the $1/V_{\rm max}$-estimated abundances over the range $10.4 \leqslant \log_{10}(M_{\rm stars}/\,h^{-2}\,{\rm M}_\odot) \leqslant 11.4$. A χ^2 fit is then performed to determine the best-fitting Schechter functions. This latter fit is carried out over larger ranges of stellar masses. For the J-inferred case, galaxies within $10.0 \leqslant \log_{10}(M_{\rm stars}/\,h^{-2}\,{\rm M}_\odot) \leqslant 11.4$ are used, and this is extended to $9.5 \leqslant \log_{10}(M_{\rm stars}/\,h^{-2}\,{\rm M}_\odot) \leqslant 11.4$ for the $r_{\rm F}$-inferred function. Also listed are the mean universal stellar mass densities derived from the SWML functions. Only statistical uncertainties are quoted. More important systematic uncertainties are discussed in the text. The final column contains the corrected estimates of the mean stellar density, taking into account the overestimation described in Section 5. Note that these stellar masses are all derived under the assumption that a Kennicutt IMF is universally applicable.

Band	$M_*/(h^{-2}\,{\rm M}_\odot)$	α	$\phi_*/(h^{-1}\,{\rm Mpc})^{-3}$	$\Omega_{\rm stars}h$	$\Omega_{\rm stars,c}h$
$M_{\rm stars}(r_{\rm F})$	$(2.78 \pm 0.11) \times 10^{10}$	-0.95 ± 0.02	$(1.19 \pm 0.04) \times 10^{-2}$	$(1.23 \pm 0.01) \times 10^{-3}$	$(1.18 \pm 0.01) \times 10^{-3}$
$M_{\rm stars}(J)$	$(4.92 \pm 0.15) \times 10^{10}$	-0.56 ± 0.04	$(1.40 \pm 0.07) \times 10^{-2}$	$(1.32 \pm 0.06) \times 10^{-3}$	$(1.04 \pm 0.05) \times 10^{-3}$

Table 4. The recovered stellar mass functions from the real data, uncorrected for the measurement bias described in the text. The units of stellar mass are $h^{-2}\,{\rm M}_\odot$ and the quoted abundances are ${\rm d}n/{\rm d}\log_{10}(M_{\rm stars})$ in $(h^{-1}\,{\rm Mpc})^{-3}$. To correct for the bias introduced by the uncertainties in estimating J-band stellar masses, applying a global shift of -0.1 in $\log_{10}(M_{\rm stars})$ is a good approximation. The $r_{\rm F}$-band results are almost unbiased, and thus do not require this correction.

$\log_{10}(M_{\rm stars})$	$r_{\rm F}$ band	J band
9.0	$(3.44 \pm 0.24) \times 10^{-2}$	$(1.47 \pm 0.44) \times 10^{-2}$
9.1	$(3.05 \pm 0.27) \times 10^{-2}$	$(1.46 \pm 0.29) \times 10^{-2}$
9.2	$(2.82 \pm 0.24) \times 10^{-2}$	$(1.42 \pm 0.30) \times 10^{-2}$
9.3	$(2.59 \pm 0.19) \times 10^{-2}$	$(1.13 \pm 0.24) \times 10^{-2}$
9.4	$(2.40 \pm 0.16) \times 10^{-2}$	$(1.21 \pm 0.25) \times 10^{-2}$
9.5	$(2.23 \pm 0.15) \times 10^{-2}$	$(1.22 \pm 0.17) \times 10^{-2}$
9.6	$(2.18 \pm 0.17) \times 10^{-2}$	$(1.33 \pm 0.09) \times 10^{-2}$
9.7	$(1.97 \pm 0.14) \times 10^{-2}$	$(1.54 \pm 0.14) \times 10^{-2}$
9.8	$(1.86 \pm 0.14) \times 10^{-2}$	$(1.22 \pm 0.15) \times 10^{-2}$
9.9	$(1.86 \pm 0.13) \times 10^{-2}$	$(1.44 \pm 0.08) \times 10^{-2}$
10.0	$(1.77 \pm 0.15) \times 10^{-2}$	$(1.49 \pm 0.12) \times 10^{-2}$
10.1	$(1.56 \pm 0.12) \times 10^{-2}$	$(1.39 \pm 0.12) \times 10^{-2}$
10.2	$(1.50 \pm 0.12) \times 10^{-2}$	$(1.33 \pm 0.10) \times 10^{-2}$
10.3	$(1.40 \pm 0.09) \times 10^{-2}$	$(1.32 \pm 0.08) \times 10^{-2}$
10.4	$(1.21 \pm 0.09) \times 10^{-2}$	$(1.36 \pm 0.08) \times 10^{-2}$
10.5	$(9.87 \pm 0.70) \times 10^{-3}$	$(1.15 \pm 0.08) \times 10^{-2}$
10.6	$(7.03 \pm 0.49) \times 10^{-3}$	$(1.02 \pm 0.07) \times 10^{-2}$
10.7	$(4.50 \pm 0.25) \times 10^{-3}$	$(7.12 \pm 0.44) \times 10^{-3}$
10.8	$(2.94 \pm 0.10) \times 10^{-3}$	$(4.60 \pm 0.24) \times 10^{-3}$
10.9	$(1.62 \pm 0.18) \times 10^{-3}$	$(3.04 \pm 0.21) \times 10^{-3}$
11.0	$(7.78 \pm 0.94) \times 10^{-4}$	$(1.64 \pm 0.11) \times 10^{-3}$
11.1	$(3.44 \pm 0.46) \times 10^{-4}$	$(8.36 \pm 0.66) \times 10^{-4}$
11.2	$(1.63 \pm 0.23) \times 10^{-4}$	$(3.67 \pm 0.31) \times 10^{-4}$
11.3	$(4.16 \pm 1.23) \times 10^{-5}$	$(1.50 \pm 0.24) \times 10^{-4}$
11.4	$(9.89 \pm 4.19) \times 10^{-6}$	$(3.75 \pm 1.22) \times 10^{-5}$
11.5	$(8.31 \pm 4.94) \times 10^{-6}$	$(1.52 \pm 1.01) \times 10^{-5}$

mass-to-light ratio. A steeper trend is seen in the $r_{\rm F}$-inferred stellar mass-to-light ratio than in the J-band one. This is because for the less luminous groups, the $r_{\rm F}$ measurements include groups with no galaxies that are detected in the near-infrared, and these groups preferentially have their stellar masses underestimated, thus dragging down the median $r_{\rm F}$-inferred stellar mass-to-light ratios.

Very similar trends are apparent in the real 2PIGG data, with a small offset to higher mass-to-light ratios relative to the mock. For the largest 2PIGGs, the stellar mass-to-light ratio is $\sim 0.47(0.62)\Upsilon_\odot$ for the $r_{\rm F}\,(J)$-band-inferred stellar masses. However, if one assumes that these are biased by the same factors as in the mock catalogue, then one should expect that the underlying stellar mass-to-light ratio in the most luminous 2PIGGs should be $\sim 0.49(0.53)\Upsilon_\odot$.

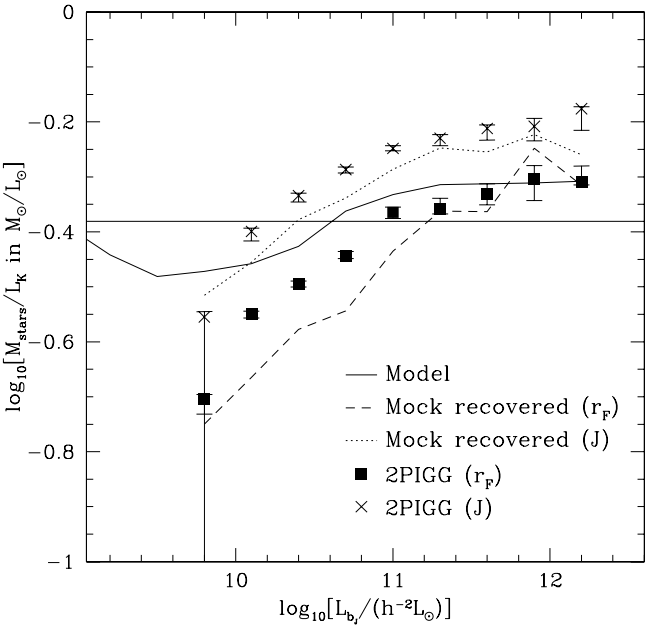

Figure 12. Stellar mass-to-light ratios ($K_{\rm S}$ band) in the groups. The horizontal line shows the mean value in the model, and the solid curve shows the variation of the median with group size present in the model. Dashed and dotted lines trace the results recovered from the mock catalogues using $r_{\rm F}$- and J-inferred stellar masses, respectively. The corresponding median values in the 2PIGG sample are shown with filled squares and crosses. Taking the median group total mass-to-light ratio of Eke et al. (2004b) maps the following luminosities $\log_{10}[L_{b_{\rm J}}/(h^{-2}\,{\rm L}_\odot)] = (10, 11, 12)$ to masses $\log_{10}[{\rm M}_\odot/(h^{-1}\,{\rm M}_\odot)] = (12.0, 13.6, 14.7)$.

These stellar mass-to-light ratios are lower than was assumed by LMS03 ($\sim 0.8\Upsilon_\odot$ for the richest clusters). This value was derived from dynamical data coupled to a maximum stellar mass model, so it represents an upper limit on the stellar mass-to-light ratio. Alternatively, if the Kennicutt IMF were changed to one producing more stellar mass at a given luminosity (for instance the 'diet' Salpeter IMF of Bell & de Jong 2001), then the stellar mass-to-light ratio found here could be increased substantially to agree with that assumed by LMS03.

7.2 Group stellar mass fractions

Fig. 13 shows how the group stellar mass fractions (i.e. the mass currently in stars divided by the total group mass) depend on group size for the $r_{\rm F}$- and J-inferred stellar masses. The horizontal line shows the mean stellar mass fraction in the model universe, and the other

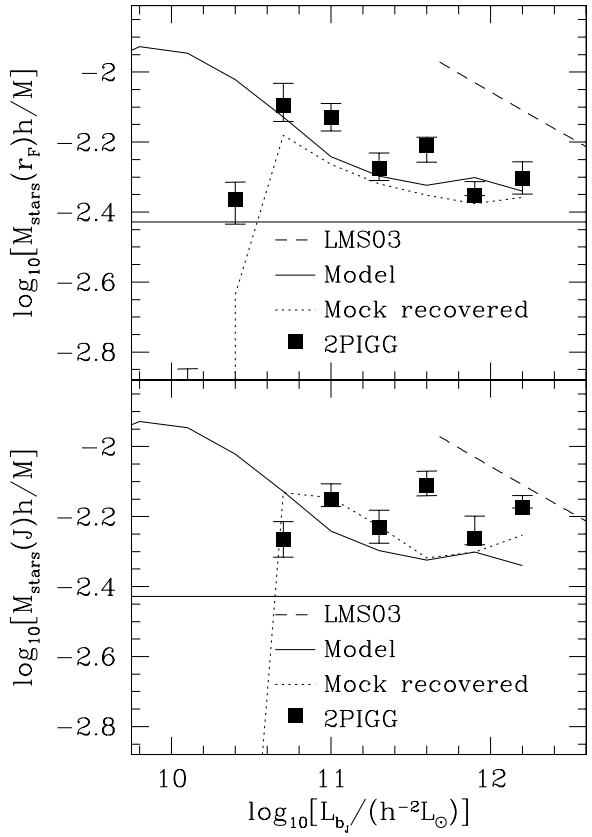

Figure 13. The ratio of stellar to total dynamical mass inferred using the r_F- (upper panel) and J-band (lower panel) estimators. A horizontal line shows the ratio $\Omega_{\rm stars}/\Omega_{\rm m}$ in the model, and the solid curve traces the variation of the median stellar mass fraction with group size in the model according to the semi-analytical prediction. A dotted line follows the results recovered from the mock catalogue, and the points show the median behaviour found in the 2PIGG sample. The dashed line traces the results found by LMS03.

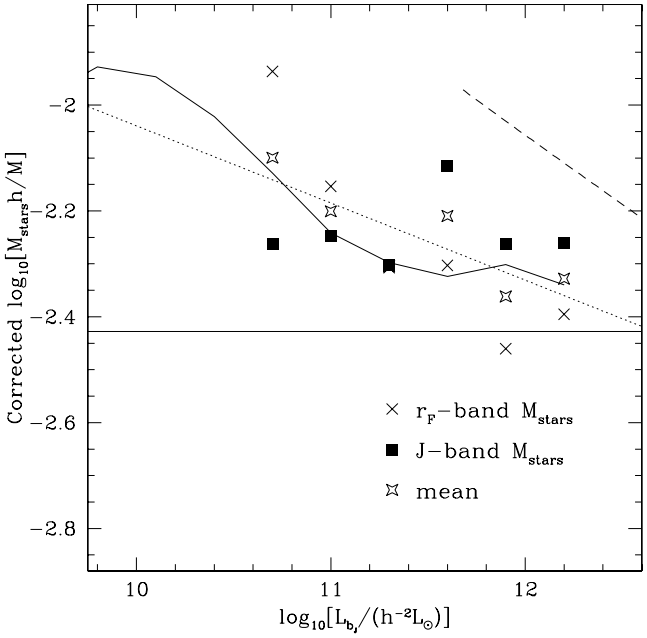

Figure 14. Corrected stellar mass fractions in the real data (symbols), compared with the model (solid line). The dotted line is a least-squares fit to the stars, and the dashed line shows the results of LMS03.

solid line traces the variation in stellar mass fraction with group size in the model, parametrized through the total group b_J-band luminosity. The median values recovered from the mock catalogues are shown with a dotted line. In constructing this curve, only groups with $z < z_{\rm max} = 0.02 + 0.04[\log_{10}(L_{b_J}/h^{-2}\,{\rm L}_\odot) - 10]$ are used. About 100 groups contribute to the bin with $\log_{10}[L_{b_J}/(h^{-2}\,{\rm L}_\odot)] = 11$ and $\sim$25 groups to the bin at $\log_{10}[L_{b_J}/(h^{-2}\,{\rm L}_\odot)] = 11.9$. For groups with $\log_{10}[L_{b_J}/(h^{-2}\,{\rm L}_\odot)] \geqslant 10.7$ the variation of stellar mass fraction is recovered well, albeit with a small offset resulting largely from the slightly different biases of the two different stellar mass estimates. This trend of increasing stellar mass fraction with decreasing group size is apparent in both the model and the mock catalogue, although the trend is more convincingly seen with the r_F-inferred stellar masses rather than those using the J-band measurements. The 2PIGG data points show a generally similar behaviour to that in the mock catalogue. Once again, a significant trend of increasing mass fraction with decreasing group size is present in the r_F-band results, although not in the J-band case.

The dashed lines in Fig. 13 show the results of LMS03, decreased by 20 per cent to mimic the effect of including a k-correction (see Lin, Mohr & Stanford 2004, for details). They measure the mass fraction within a smaller radius than is used to define groups here. Thus, to calculate where their results fit on these plots, it has been necessary to assume a conversion from their M_{500} to virial mass, $M_{\rm vir}$ (this is taken simply as a factor 1.9 for a typical cluster dark matter density profile with a concentration $c_\Delta = 5$), to use the typical mass-to-b_J-band light as a function of group size found by Eke et al. (2004b), and to account for their use of h_{70}. For the largest clusters, they find a stellar mass fraction of $\sim 8 \times 10^{-3}\,h^{-1}$, in contrast to the $\sim 5.0(6.7) \times 10^{-3}\,h^{-1}$ found here using the $r_F(J)$-band stellar masses. This is similar to the difference between the stellar mass-to-light ratios in the two studies.

Interestingly, the variation of stellar mass fraction with cluster size found by LMS03 exceeds that found here, despite their clusters being in a region where no significant trend is apparent in the 2PIGG results. This is reminiscent of the situation with the total mass-to-light ratio comparison. In fact, the 2PIGG results would show only weak evidence of any trend if it were not for the data at $\log_{10}[L_{b_J}/(h^{-2}\,{\rm L}_\odot)] \lesssim 11$ in the upper panel of Fig. 13. One could envisage that a strong trend of decreasing stellar mass fraction with increasing total mass could be artificially created if the lowest mass clusters preferentially had their masses underestimated.

Under the assumption that the real mass fractions are biased in the same way as those in the mock catalogue, a corrected stellar mass fraction can be derived. Fig. 14 shows a comparison between the model from which the mock was created and the corrected results for the real data. The different symbols show the two different stellar mass estimates and the mean (in log space) of these two. A dotted line traces the least-squares fit to the mean values. This line has the equation

$$\log_{10}(M_{\rm stars}h/M) = -0.58 - 0.146\,\log_{10}\left[L_{b_J}/\left(h^{-2}\,{\rm L}_\odot\right)\right]. \quad (7.1)$$

For the biggest clusters, the typical corrected stellar mass fraction is only $\sim 5 \times 10^{-3}\,h^{-1}$.

8 WHERE ARE THE STARS?

Having determined both the total stellar mass function of galaxies and the variation of stellar mass content with group size, the next

natural step is to determine how all stars are partitioned among groups. It should be noted that this work only considers stars that are associated with galaxies, ignoring any population of intergalactic stars. In large galaxy clusters, a few tens of per cent of the total cluster stellar mass may reside in intergalactic stars (e.g. Zibetti & White 2004; Lin & Mohr 2004). However, only a small fraction of all stars reside in such large clusters, as will be shown.

To determine the fraction of stars in groups of a given luminosity, a trivariate SWML method has been used. By choosing group luminosity to describe the group size, rather than mass, it is possible to use groups containing only a single galaxy. These contribute a significant fraction of the galaxies, and hence stellar mass, and are thus crucial in forming a full picture of where all of the stars reside. The trivariate SWML method extends the method used in the previous sections by adding an extra variable, namely, the luminosity of the group in which any particular galaxy exists. Following the nomenclature of Loveday (2000), the space density of galaxies, $\phi(L_{\rm g}, L, M)$, with luminosity L, stellar mass M and residing in a group with total $b_{\rm J}$ luminosity $L_{\rm g}$, can be used to write the probability of galaxy i taking particular values as

$$p_i = \frac{\phi\left(L^i_{\rm g}, L^i, M^i\right)}{\int_{L^i_{\rm g,min}}^{\infty} \int_{L^i_{\rm min}}^{L^i_{\rm max}} \int_0^{\infty} \phi(L_{\rm g}, L, M)\, {\rm d}L_{\rm g}{\rm d}L{\rm d}M}. \quad (8.1)$$

The lower integration limit for the group total $b_{\rm J}$ luminosity will exceed that for the galaxy luminosity, because of the group luminosity that lies in galaxies beneath the flux limit of the 2dFGRS. This extra luminosity is calculated assuming that group galaxies follow the Schechter function determined by Norberg et al. (2002) for the entire population (as was done by Eke et al. 2004b when defining group luminosity). The galaxy luminosity and stellar mass variables are either $b_{\rm J}$-band luminosity and $r_{\rm F}$-band stellar mass or J-band luminosity and stellar mass. As shown by the integration limits, all stellar masses are accessible at any given galaxy luminosity – this was also assumed for the bivariate case earlier. Performing the usual operations to maximize this probability while describing the galaxy space density in a stepwise manner leads to the following estimate of the density of galaxies residing in groups with

$$L^j_{\rm g} - \Delta L_{\rm g}/2 < L_{\rm g} \leqslant L^j_{\rm g} + \Delta L_{\rm g}/2, \quad (8.2)$$

having luminosity

$$L^k - \Delta L/2 < L \leqslant L^k + \Delta L/2, \quad (8.3)$$

and stellar mass

$$M^l - \Delta M/2 < M \leqslant M^l + \Delta M/2: \quad (8.4)$$

$$\phi_{jkl} = \frac{n_{jkl}}{\sum_{i=1}^{N} \left(\frac{H_{ijkl}\Delta L_{\rm g}\Delta L\Delta M}{\sum_{p=1}^{N_{L_{\rm g}}} \sum_{q=1}^{N_L} \sum_{r=1}^{N_M} \phi_{pqr} H_{ipqr} \Delta L_{\rm g}\Delta L\Delta M} \right)}. \quad (8.5)$$

n_{jkl} represents the total number of galaxies in bin (j, k, l) and H_{ipqr} is a trivariate version of the ramp function as described by Loveday (2000). $N_{L_{\rm g}}$, N_L and N_M are the numbers of bins in group luminosity, galaxy luminosity and galaxy stellar mass, respectively.

The trivariate function can be projected to recover the galaxy luminosity function or the stellar mass function, for example. However, by projecting along the individual galaxy luminosity and stellar mass directions, the distribution of stars among groups of different luminosity can be retrieved.

Fig. 15 shows both the differential and the cumulative distributions of stellar mass among different-sized groups. While the distributions recovered from the mock catalogue are quite similar to that present in the model, there is a trend in the mock of placing a higher fraction of the stars in larger groups as the upper redshift of the sample is increased. This is particularly apparent for the $r_{\rm F}$-band results, because the mock J-band sample is also restricted by the relatively high 2MASS flux limit. For the $z < 0.05$ samples, a lack of large local clusters in the mock catalogue means that the results significantly underestimate the fraction of all stars in groups with $\log_{10}(L_{b_{\rm J}}) > 11$. As the upper redshift limit is increased, the volume encloses a fairer sample of the mock universe. Furthermore, the correction for missing group luminosity increases, which leads to an overestimate of the abundance of the more luminous groups. Consequently, the stellar mass is too frequently assigned to larger groups than should be the case. To correct for these systematic biases, one can choose an upper redshift that varies with group luminosity. The points in Fig. 15 show how the redshift limit can be chosen so that the model distribution is very accurately recovered. When the cut on group luminosity at a given redshift is introduced, it is necessary to alter the lower limit for the group luminosity integration in equation (8.1).

Assuming that similar systematic biases are appropriate in both the mock and real data, the points in the bottom row of Fig. 15 should represent unbiased estimates of the distribution of stellar mass among 2PIGG groups. The $r_{\rm F}$-band curves are very similar to those recovered from the mock catalogue, with the main differences being that the real Universe contains a higher fraction of stars in very small groups and groups with $\log_{10}(L_{b_{\rm J}}) \sim 10$. The model stars are more frequently placed in groups with $\log_{10}(L_{b_{\rm J}}) \sim 9$–$9.5$ than is the case in the real Universe. The difference for the smallest groups can be understood by recalling that the mock catalogue did not include galaxies with $M_{b_{\rm J}} > -16$. With these very low-luminosity galaxies missing, fewer stars are placed into the smallest groups. In the J band, the results are broadly similar to the $r_{\rm F}$ band, with a slight deficit of stars in small groups. This reflects the difference in faint-end slopes of the $r_{\rm F}$-inferred and J-inferred stellar mass functions shown in Fig. 11, at least some of which results from the fact that 2MASS misses some low surface brightness galaxies (Andreon 2002; Bell et al. 2003). As this additional systematic bias is known to affect the J-band results, the following fit is provided only for the $r_{\rm F}$-inferred stellar mass distribution:

$$f(M_{\rm stars})(>L_{b_{\rm J}}) = 1 - \int_{-\infty}^{\log_{10} L_{b_{\rm J}}} \frac{\exp\left[\frac{(x-\bar{x})^2}{2\sigma^2}\right]}{\sqrt{2\pi\sigma^2}}\, {\rm d}x, \quad (8.6)$$

where $\sigma = 0.94$ and $\bar{x} = 10.37$. This fit to the fraction of stellar mass in haloes with a total blue luminosity exceeding $L_{b_{\rm J}}$ is accurate to better than 0.02 for all group luminosities.

9 CONCLUSIONS

The near-IR light and stellar content of the Universe as a whole, and its constituent groups, have been quantified using the 2dFGRS, the 2PIGG catalogue and the 2MASS. This work extends that of previous studies with the largest sets of galaxies and groups yet used for these purposes. Furthermore, the mock galaxy catalogues that have been employed allow a careful quantification of the systematic errors associated with estimating stellar masses. This represents an important advance, because the systematic bias introduced by errors in the estimated stellar masses, which has been quantified via the mock catalogues, is sufficiently large that the mean stellar mass density had previously been significantly overestimated. The mock catalogues permit this bias to be quantified and corrected for.

The mean luminosity density in the Universe is found to be $\bar{\rho}_J = (3.57 \pm 0.11) \times 10^8\, h\, {\rm L}_\odot\, {\rm Mpc}^{-3}$ and $\bar{\rho}_{K_{\rm S}} = (7.04 \pm 0.23) \times 10^8\, h\, {\rm L}_\odot\, {\rm Mpc}^{-3}$ (statistical uncertainty only) in the two near-IR bands considered here. Systematic uncertainties are likely to be of

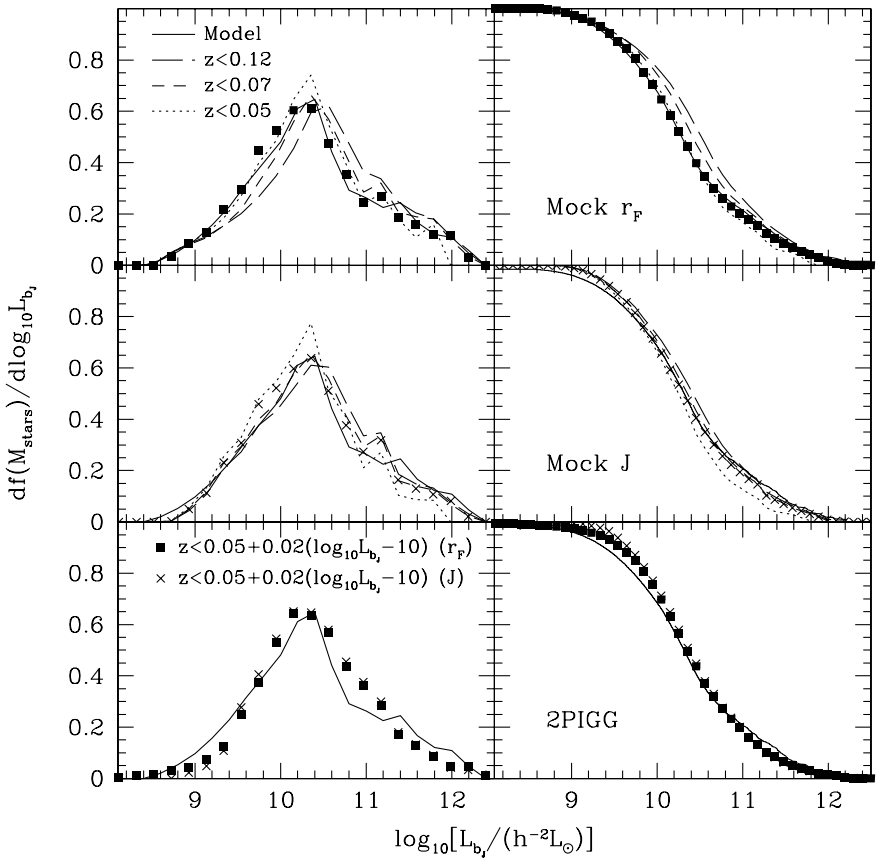

Figure 15. The fraction of all stellar mass within groups as a function of group size, parametrized by group b_J-band luminosity. Differential and the corresponding cumulative distributions are shown in the left and right columns, respectively. The solid line in each panel shows the model distribution, while the other curves in the top two rows trace the estimates recovered as the maximum redshift is changed from 0.05 (dotted) to 0.07 (short dashed) and 0.12 (long dashed). Results of using r_F-inferred stellar masses in the mock catalogue are shown in the top row, whereas the middle row contains the J-inferred stellar masses. The symbols show the estimates with a variable upper redshift limit, dependent on the total group b_J-band luminosity, as quantified in the legend. The bottom row shows the 2PIGG results, with the variable upper redshift limits for both the r_F- and J-inferred stellar mass estimates, as well as the reference model. Taking the median group total mass-to-light ratio of Eke et al. (2004b) maps the following luminosities $\log_{10}[L_{b_J}/(h^{-2}\,\mathrm{L}_\odot)] = (10, 11, 12)$ to masses $\log_{10}[\mathrm{M}_\odot/(h^{-1}\,\mathrm{M}_\odot)] = (12.0, 13.6, 14.7)$.

the order of 20 per cent and dominated by the completeness of the catalogues used and the conversion of Kron to total magnitudes. Taking into account the bias in the stellar mass density that, according to the mock catalogues, arises from the uncertainty in inferring stellar masses from galaxy fluxes and colours, the mean stellar mass density amounts to $\Omega_{\rm stars}h = (1.11 \pm 0.05) \times 10^{-3}$. This value assumes that a Kennicutt IMF is applicable to all sites of star formation. If a Salpeter IMF had been chosen then the estimated $\Omega_{\rm stars}h$ would be a factor of $\sim$2.1 larger. The value of $\Omega_{\rm stars}\,h$ provides a measure of the density of material currently locked up in stars. In conjunction with knowledge about what fraction of stellar mass is recycled, this gives a constraint on the integral over time of the universal star formation rate.

The stellar mass-to-light ratio and stellar mass fraction are both studied as functions of 2PIGG size. Rich clusters are found to have stellar mass-to-K_S band light ratios of $\sim 0.55\Upsilon_\odot$, a value that is about 60 per cent larger than that found to be typical of groups with $\log_{10}[L_{b_J}/(h^{-2}\,\mathrm{L}_\odot)] = 10$. Removing the systematic errors inherent in this determination reduces the cluster value to $0.50\Upsilon_\odot$. The opposite trend is found for the stellar mass fraction, with larger groups having smaller values. Taking into account the systematic error in the recovery gives a typical stellar mass fraction of $\sim 5 \times 10^{-3}\,h^{-1}$ for the richest clusters.

Finally, a trivariate stepwise maximum likelihood method is employed to partition, into groups of different size, the stellar mass that resides in galaxies in the local Universe. It is found that only a couple of per cent of this stellar mass resides in galaxy clusters with $\log_{10}[L_{b_J}/(h^{-2}\,\mathrm{L}_\odot)] > 12$ ($\log_{10}[M/(h^{-1}\,\mathrm{M}_\odot)] \gtrsim 14.7$). Half of this stellar mass is located in groups with $\log_{10}[L_{b_J}/(h^{-2}\,\mathrm{L}_\odot)] > 10.4$ ($\log_{10}[M/(h^{-1}\,\mathrm{M}_\odot)] \gtrsim 12.5$). Once again, using mock catalogues can reduce the systematic biases associated with the entire measurement procedure. This adds weight to the assertion that the measured distribution is an accurate representation of the true underlying distribution of stellar mass among different-sized haloes and, as such, represents a valuable link in the chain connecting theory with observation.

ACKNOWLEDGMENTS

We would like to thank the anonymous referee for comments that significantly improved the content of this paper. VRE and CMB are Royal Society University Research Fellows. HMK was supported by a Royal Society Summer Studentship. JAP is a PPARC senior research fellow. This work was supported by a PPARC rolling grant for Extragalactic Astronomy and Cosmology. The 2dF Galaxy Redshift Survey was made possible through the dedicated efforts of the staff

of the Anglo-Australian Observatory, both in creating the 2dF instrument and in supporting it on the telescope. The 2dFGRS team is also acknowledged for its efforts in producing the survey. This publication makes use of data products from the Two Micron All-Sky Survey, which is a joint project of the University of Massachusetts and the Infrared Processing and Analysis Center/California Institute of Technology, funded by the National Aeronautics and Space Administration and the National Science Foundation.

REFERENCES

Andreon S., 2002, A&A, 382, 495
Bell E. F., de Jong R. S., 2001, ApJ, 550, 212
Bell E. F., McIntosh D. H., Katz N., Weinberg M. D., 2003, ApJS, 149, 289
Bruzual G., Charlot S., 2003, MNRAS, 334, 1000
Cole S., Lacey C. G., Baugh C. M., Frenk C. S., 2000, MNRAS, 319, 168
Cole S. et al. (The 2dFGRS Team), 2001, MNRAS, 326, 255 (C01)
Colless M. et al. (The 2dFGRS Team), 2001, MNRAS, 328, 1039
Colless M. et al. (The 2dFGRS Team), 2003, astro-ph/0306581
Cross N. J. G., Driver S. P., Liske J., Lemon D. J., Peacock J. A., Cole S., Norberg P., Sutherland W. J., 2004, MNRAS, 349, 576
Driver S. P., Liske J., Cross N. J. G., De Propris R., Allen P. D., 2005, MNRAS, 360, 81
Drory N., Bender R., Hopp U., 2004, ApJ, 616, L103
Efstathiou G., Ellis R. S., Peterson B. A., 1988, MNRAS, 232, 431
Eke V. R. et al. (The 2dFGRS Team), 2004a, MNRAS, 348, 866
Eke V. R. et al. (The 2dFGRS Team), 2004b, MNRAS, 355, 769
Jarrett T. H., Chester T., Cutri R., Schneider S., Skrutskie M., Huchra J. P., 2000, AJ, 119, 2498
Jenkins A. et al., 1998, ApJ, 499, 20
Kennicutt R. C., 1983, ApJ, 272, 54
Kochanek C. S. et al., 2001, ApJ, 560, 566
Kochanek C. S., White M., Huchra J., Macri L., Jarrett T. H., Schneider S. E., Mader J., 2003, ApJ, 585, 161
Lin Y.-T., Mohr J. J., 2004, ApJ, 617, 879
Lin Y.-T., Mohr J. J., Stanford S. A., 2003, ApJ, 591, 749 (LMS03)
Lin Y.-T., Mohr J. J., Stanford S. A., 2004, ApJ, 610, 745
Loveday J., 2000, MNRAS, 312, 557
Navarro J. F., Frenk C. S., White S. D. M., 1997, ApJ, 490, 493 (NFW)
Norberg P. et al. (The 2dFGRS Team), 2002, MNRAS, 336, 907
Rines K., Geller M. J., Diaferio A., Kurtz M. J., Jarrett T. H., 2004, AJ, 128, 1078
Salpeter E. E., 1955, ApJ, 121, 161
Schechter P., 1976, ApJ, 203, 297
Sodré L., Lahav O., 1993, MNRAS, 260, 285
Zibetti S., White S. D. M., 2004, in Diaferio A., ed., Proc. IAU Colloq. 195, Outskirts of Galaxy Clusters: Intense Life in the Suburbs (astro-ph/0404326)

This paper has been typeset from a TEX/LATEX file prepared by the author.